

1N-34

181583

p-37

NASA Contractor Report 191477

ICASE Report No. 93-28

ICASE



INTERACTING SCALES AND ENERGY TRANSFER IN ISOTROPIC TURBULENCE

Ye Zhou

(NASA-CR-191477) INTERACTING
SCALES AND ENERGY TRANSFER IN
ISOTROPIC TURBULENCE Final Report
(ICASE) 37 p

N94-13133

Unclas

G3/34 0181583

NASA Contract No. NAS1-19480

June 1993

Institute for Computer Applications in Science and Engineering

NASA Langley Research Center

Hampton, Virginia 23681-0001

Operated by the Universities Space Research Association



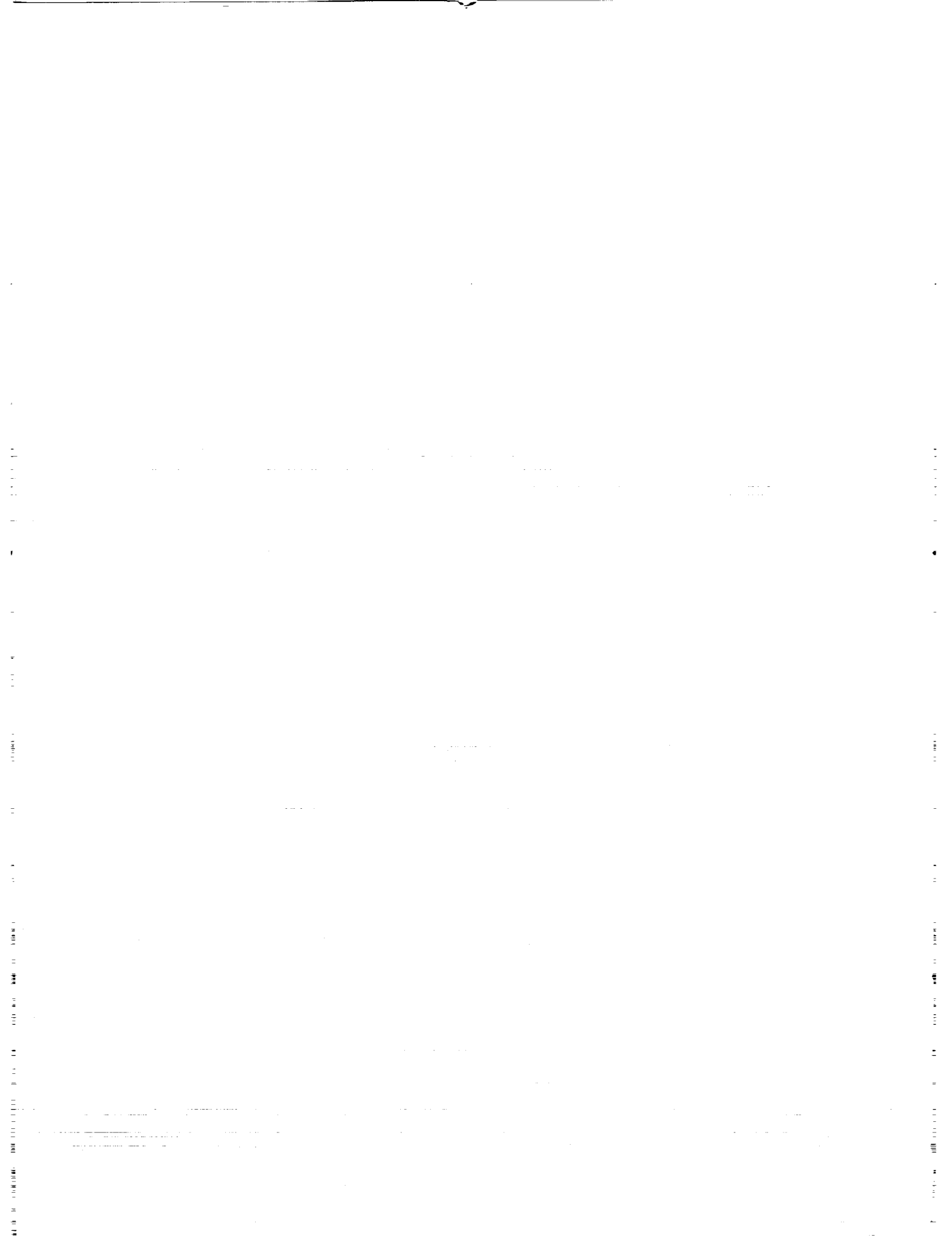
National Aeronautics and
Space Administration

Langley Research Center
Hampton, Virginia 23681-0001



ICASE Fluid Mechanics

Due to increasing research being conducted at ICASE in the field of fluid mechanics, future ICASE reports in this area of research will be printed with a green cover. Applied and numerical mathematics reports will have the familiar blue cover, while computer science reports will have yellow covers. In all other aspects the reports will remain the same; in particular, they will continue to be submitted to the appropriate journals or conferences for formal publication.



INTERACTING SCALES AND ENERGY TRANSFER IN ISOTROPIC TURBULENCE

Ye Zhou¹

Institute for Computer Applications in Science and Engineering
NASA Langley Research Center
Hampton, VA 23681-0001

ABSTRACT

The dependence of the energy transfer process on the disparity of the interacting scales is investigated in the inertial and far-dissipation ranges of isotropic turbulence. The strategy for generating the simulated flow fields and the choice of a disparity parameter to characterize the scaling of the interactions is discussed. The inertial range is found to be dominated by relatively local interactions, in agreement with the Kolmogorov assumption. The far-dissipation is found to be dominated by relatively non-local interactions, supporting the classical notion that the far-dissipation range is slaved to the Kolmogorov scales. The measured energy transfer is compared with the classical models of Heisenberg [*Z. Physik*, **124**, 628, (1948)], Obukhov [*Isv. Geogr. Geophys. Ser.*, **13**, 58, (1949)] and the more detailed analysis of Tennekes and Lumley [*The First Course of Turbulence*, MIT press, (1972)]. The energy transfer statistics measured in the numerically simulated flows are found to be nearly self-similar for wavenumbers in the inertial range. Using the self-similar form measured within the limited scale range of the simulation, we construct an 'ideal' energy transfer function and the corresponding energy flux rate for an inertial range of infinite extent. From this flux rate we calculate the Kolmogorov constant to be 1.5, in excellent agreement with experiments [A.S. Monin and A.M. Yaglom, *Statistical Fluid Mechanics*, Vol. 2, MIT Press, (1975)].

¹The majority of this work was completed at the Center for Turbulence Research, Stanford University, Stanford, CA 94305, and NASA Ames Research Center, Moffet Field, CA 94305. Research was supported by the National Aeronautics and Space Administration under NASA Contract No. NAS1-19480 while the author was in residence at the Institute for Computer Applications in Science and Engineering, NASA Langley Research Center, Hampton, VA 23681.

1. Introduction

Recently, an entire volume of the *Proceedings of the Royal Society*¹ was devoted to Kolmogorov's ideas about turbulence. Indeed, Kolmogorov's inertial range theory²⁻⁴ has formed a foundation for turbulence research for the last fifty years even though the existence of an inertial range requires high Reynolds numbers (Re) normally encountered only in geophysical flows⁴⁻⁵.

Almost all turbulence theories and models rely on assumptions about the energy transfer process. Although experiments can measure the total energy transferred to a given scale from all other scales of turbulent motion, it is very difficult for them to observe the details of the energy transfer process. On the other hand, analytical theories are not fully satisfactory since they already involve certain assumptions about triad interactions (Domaradzki and Rogallo⁶). A promising approach to this question is through the use of results from numerical simulations. High resolution direct numerical simulation (DNS) of turbulence allows precise measurements of the individual terms of the Navier-Stokes equation, and is now a well established adjunct to experiment for testing various theoretical predictions. Recently, the classical Kolmogorov picture of energy transfer was questioned by Domaradzki and Rogallo⁶, Yeung and Brasseur⁷ and Ohkitani and Kida⁸ who concluded from low Reynolds-number numerical simulations that energy is transferred downscale locally, supporting the basic concept leading to the inertial range. However, they also concluded that this local energy transfer resulted from nonlocal interactions, a notion clearly at variance with the classical Kolmogorov picture. Yueng and Brasseur⁷ further argued that the predominance of the nonlocal interactions would also invalidate the Kolmogorov assumption of local isotropy at small scales.

It is important to stress that the Kolmogorov theory is valid only for very high Reynolds number turbulent flows. Measurements obtained from low Reynolds number simulations, and also from large-eddy-simulations in which closure models are used, must be interpreted with great caution regarding their implications about the Kolmogorov theory. While we have no disagreement with these studies concerning the actual measurement of the raw interaction statistics—the triad nonlinear transfer $T(k, p, q)$ —we believe that $T(k, p, q)$ is not the appropriate quantity from which to determine whether the nonlinear interactions contributing to the energy transfer are local or not. Rather, we follow Kraichnan's argument⁹ that these raw interaction statistics should be viewed only as a mathematical building block in the energy transfer process and their *physical* interpretation requires further summation, during which much additional cancellation occurs.

2. The basic equations and measurements

We are concerned here with isotropic turbulence in an incompressible fluid. The velocity field $u_\alpha(\mathbf{k}, t)$ in the spectral space is governed by the Navier-Stokes equation

$$\left[\frac{\partial}{\partial t} + \nu k^2\right]u_\alpha(\mathbf{k}, t) = -\frac{i}{2}P_{\alpha\beta\gamma}(k) \sum_{\mathbf{p}+\mathbf{q}=\mathbf{k}} u_\beta(\mathbf{p}, t)u_\gamma(\mathbf{q}, t) + f_\alpha(\mathbf{k}, t), \quad (1)$$

where $P_{\alpha\beta\gamma}(k) = k_\beta P_{\alpha\gamma}(k) + k_\gamma P_{\alpha\beta}(k)$, $P_{\alpha\beta}(k) = \delta_{\alpha\beta} - k_\alpha k_\beta / k^2$, f is the external force ($f = 0$ for the decaying case), and ν is the kinematic viscosity.

The equation for the energy spectrum $E(k) = 4\pi k^2 \langle \frac{1}{2}|u(\mathbf{k})|^2 \rangle$ is

$$\left[\frac{\partial}{\partial t} + 2\nu k^2\right]E(k) = T(k) + F(k), \quad (2)$$

where $F(k)$ is the forcing spectrum, $T(k)$ is the the energy transfer function, and $\langle \dots \rangle$ denotes averaging over spherical shells. The contribution to $T(k)$ resulting from nonlinear interactions between Fourier modes in wavenumber band k and those in bands p and q is denoted by $T(k, p, q)$, which follows directly from (1) as

$$T(k, p, q) = \frac{1}{2} \sum \text{Im}[u_\alpha(\mathbf{k})P_{\alpha\beta\gamma}(k)u_\beta(\mathbf{p})u_\gamma(\mathbf{q})]. \quad (3)$$

Here \sum denotes summation over spherical shells in $\mathbf{k}, \mathbf{p}, \mathbf{q}$ subject to the triangle constraint $\mathbf{k} = \mathbf{p} + \mathbf{q}$. In turn, the net energy transfer into band k is the result of all contributing interactions:

$$T(k) = \sum_{p,q} T(k, p, q). \quad (4)$$

3. The simulated flow fields

Homogeneous turbulence at high Reynolds number is characterized by four different ranges of spatial scales:

1. The very-large scales: This range is peculiar to unbounded flows, and the degree to which its energy spectrum is universal is a subject of current study [see, for example, Chasnov¹⁰].

2. The energy containing scales: These control the overall dynamics of turbulence, and are directly responsible for turbulence transport processes.

3. The inertial subrange scales: Here the effects of forcing and dissipation can be ignored in the equation of motion. This range represents the pure energy cascade, and its energy spectrum is the well known Kolmogorov spectrum

$$E(k) = C_k \epsilon^{2/3} k^{-5/3}, \quad (5)$$

where ϵ is the energy dissipation rate, and C_k is the Kolmogorov constant.

4. The far-dissipation range. The energy spectrum decreases exponentially with k .

$$E(k) \sim \exp[-\alpha(k\eta)^m], \quad k\eta \gg 1, \quad (6)$$

where $\eta = (\nu^3/\epsilon)^{1/4}$ is the Kolmogorov length scale. The precise form, including the value of m , is also a subject of current study.

The capacity of present and foreseeable supercomputers is not adequate for fully resolved DNS at large Reynolds number, and it is not possible to resolve phenomena occurring at spatial and temporal scales extending over many orders of magnitude. Large eddy simulation (LES) is an attempt to avoid the numerical resolution of the small scale dynamics by discarding the small scales themselves, which are presumed to contain rather universal features, while retaining their effect on the resolvable scales by adding subgrid model terms, usually as a dissipative mechanism, to the resolvable scale equations of motion¹¹. Although the limitations of present day supercomputers do not allow simulation of the entire spectral space at high Reynolds number, we can perform LES and DNS, for both forced and decaying turbulence, with about two decades of spatial-scale resolution. Our strategy then is to obtain accurate databases separately for each scale range, using appropriate combinations of these approaches.

It is essential to obtain a simulated flow field as close to the Kolmogorov inertial range as possible in order to obtain accurate measurements of the transfer process. The inertial range is represented by statistically stationary flow fields generated using a Fourier spectral code in which the Kolmogorov spectrum is maintained explicitly. As a result, the energy spectrum for the inertial range LES is $k^{-5/3}$ over the entire spectral range of the simulation. The method follows the spirit of Kraichnan's constrained decimation theory¹² and is essentially that of She and Jackson¹³ who reported a simulation at 128^3 resolution (they called their method the "constrained Euler" model). Basically at each time step, the Fourier modes in each spherical shell are multiplied by the real constant that returns the shell energy to the Kolmogorov $k^{-5/3}$ spectrum. This method can be thought of as a constrained dynamical system. For an N^3 problem, one has placed $N/2$ constraints on the $2N^3$ degrees of freedom. The method is equivalent to the use of forcing at the small wavenumber (via a linear instability) and a spectral eddy viscosity at high wavenumber. To validate the method, we have repeated our analysis using the forced LES dataset of Chasnov¹⁴ at 128^3 resolution, which was generated using the traditional spectral eddy viscosity¹⁵ and a backscatter forcing, and we also performed simulations at 64^3 , 128^3 , and 256^3 to investigate the effect of mesh

size. We analysed several independent fields at each resolution and found no variation in the statistics. The results reported in this paper were measured in a stationary velocity field on a 256^3 mesh size after 3200 time steps of evolution. She and Jackson¹³ found that the measured scaling exponents for flatness factors are in good agreement with experiment¹⁶.

As in all numerical simulations, our inertial-range dataset is restricted by the finite computational domain, and separating physics from numerics becomes an important concern. It is necessary to identify and eliminate the numerical artifacts in the measurements. This effort leads to the *construction* of an ‘ideal’ Kolmogorov inertial range and a determination of the Kolmogorov constant.

The dissipation range is represented by a low-Reynolds-number forced DNS that reaches a steady statistical state and a fully developed dissipation-range energy spectrum. The form of the far-dissipation range spectrum has been of interest for a long time, and recently there has been renewed interest in the subject.

We have also examined a high-Reynolds-number decaying DNS for comparison to both the LES and the low Reynolds number DNS.

The main characteristics of these flow fields can be found in Table 1.

The energy spectrum for the high Reynolds number DNS (figure 2a) exhibits about one decade of $k^{-5/3}$ inertial range. The same spectrum, replotted in figure 2b, indicates that for $k\eta > 0.3$ the dissipation range has the form $E(k) \sim \exp(-\alpha k\eta)$ with $\alpha \sim 4.9$. Figure 2 suggests that the high Reynolds number DNS dataset is a useful supplement to the more specialized simulations of the inertial and far-dissipation ranges. The forced DNS at $R_\lambda \sim 40$ (figure 3) contains a longer resolved dissipation range, as a result of the lower Reynolds number, in which the spectrum is proportional to $\exp(-5.1k\eta)$. The α values of $4.9 \sim 5.1$ agree with those found in forced DNS by Kerr¹⁷ and Sanada¹⁸ and in decaying DNS by Kida and Murakami¹⁹. Note that the “turn up” of the spectra at very high k is the pile up of energy, a numerical artifact associated with local energy transfer cutoff by the Fourier spectral algorithm.

The transfer function at one instant of time in the inertial range LES (figure 4a) illustrates that the flow field has over one decade scale that is relatively free of end effects. The energy balances for the decaying DNS at high Reynolds number and the forced DNS at low Reynolds number (figures 4b-4c) indicate that there is an instantaneous quasi-equilibrium between transfer and dissipation for $k > 30$ (high Re decaying DNS) and $k > 20$ (low Re forced DNS), respectively. These simulated flow fields provide the data for our measurements of the energy transfer process.

4. The scale disparity parameter

This work addresses a fundamental question regarding the energy transfer process. At issue is the process of energy transfer across the spectrum and the choice of an appropriate statistical quantity to describe it. Basically the problem is that the transfer is conservative, with $T(k) < 0$ for small k and $T(k) > 0$ for large k , but since we cannot “tag” energy we can not follow its “flow” across the spectrum precisely. We quote Tennekes and Lumley²⁰:

Although we expect that there will be a net flux of energy from smaller to larger wavenumber, we do not know which eddy sizes are involved in the spectral energy transfer across a given wavenumber. For example, does the energy come from eddies that are slightly larger than a given wavelength, or does it come from all larger eddies indiscriminately? In the same way, is the energy absorbed at wave numbers slightly larger than a given value, or is it absorbed by all larger wavenumbers ?

The basic approach of obtaining the band-to-band energy transfer function $T(k, p, q)$ has been described in Domaradzki and Rogallo⁶, but here we have partitioned the spectral space into half-octave bands rather than the linear bands previously used. The logarithmic shells in our summation have introduced extra factors k, p and q . Since the turbulence is isotropic, it is natural to average over spherical $\mathbf{k}, \mathbf{p}, \mathbf{q}$ shells giving the net transfer into band k resulting from all interactions that involve bands p, q and k .

The raw interaction measurements $T(k, p, q)$, formally the transfer due to the interaction of sharply-truncated Fourier bands, form the basic building blocks for our analysis of the energy transfer process, and as figure 5 shows, they have qualitatively similar structures in all of the simulated ranges. In particular, contributions $T(k, p, q)$ to $T(k)$ for a fixed p -band is dominated by interactions with $q < p$. The plots illustrate a distinctly different character for low and high k bands. In the range $0 < k < 2p$, $T(k, p, q)$ has a pair of positive and negative peaks resulting from interactions with q in the range $0 < q < p$. These interactions, which involve little cancellation, are the major contributors to $T(k, p)$ when summed over q . In contrast for $k > 2p$ interactions involving $q > p$ produce positive and negative contributions to $T(k, p, q)$ of about the same magnitude, which tend to cancel. Thus, this latter-type of interaction does not contribute as significantly to $T(k, p)$ as the amplitudes in the figure might suggest. The degree of cancellation, and the net contribution to the transfer depends on the range involved. The contribution is significant in the far-dissipation range. Based on such raw interaction measurements, and particularly the behavior at large k , Domaradzki and Rogallo⁶, Yeung and Brasseur⁷, and Ohkitani and Kida⁸ concluded that the local energy

transfer resulted from non-local interactions. But it is apparent from figure 5 that the contributions of the various interactions nearly cancel at high k .

Using the helical wave decomposition and an “instability assumption”, Waleffe²¹ has identified which non-local helical-mode interactions are responsible for the observed large local transfers. He argued that the energy cascade due to those interactions is actually reversed in the inertial range. The analysis indicates that the physical process of the straining of small scales by large scales, which results in local transfer by nonlocal interaction, must be represented by at least two triads, resulting in cancellation between their individual triad transfers $T(k, p, q)$.

In order to separate the local and nonlocal interactions, we introduce the parameter

$$s(k, p, q) = \frac{\max(k, p, q)}{\min(k, p, q)} \quad (7)$$

which indicates directly the disparity of the interacting scales. This parameter has been used to classify interactions as local ($s \leq 2$) and nonlocal ($s > 2$) by Lesieur²². Kraichnan⁹ introduced a different set of parameters (v, w) where v ($v \leq 1$) is the ratio of the shortest to the middle leg and w is defined as k/p ($1 < w < 1+v$). The pair (v, w) completely determines a unique triad shape. Using the test field model, Kraichnan⁹ calculated an energy transfer locality function that gives the fraction of energy flux across a wavenumber due to triangles whose smallest leg is larger than v times the middle leg. Analysis of this function indicates that 65% of the transfer involves wavenumber triads in which the smallest wavenumber is less than one-half of the middle wavenumber.

The work of Kraichnan⁹ provided a theoretical criterion by which one can determine the relative importance of local and nonlocal interactions. For a given scale k , he argued that all raw interaction statistics must be summed such that physical quantities contain only *one* parameter which indicates the scale disparity of the interaction.

We use the scale disparity parameter s to study the flow of energy to small scales and determine the scaling laws for the contributions of various interactions.

5. Analysis of the energy transfer function

The net energy transfer to scale k results from interactions of various disparities s as

$$T(k) = \sum_s T(k, s), \quad (8a)$$

where

$$T(k, s) = \sum_{p, q|s} T(k, p, q) \quad (8b)$$

is the partial sum of $T(k, p, q)$, over all interactions in (p, q) at constant s . The key point here is that the summation covers all interaction scales, subject to the triangle constraint, leaving only the dependence on scale disparity. This follows in spirit the procedure described in Kraichnan⁹. This measure has the following advantage over the $T(k, p, q)$ measurements: $\int dk T(k, s) = 0$. This follows immediately from the detailed energy balance

$$T(k, p, q) + T(p, q, k) + T(q, k, p) = 0$$

and the invariance of $s(k, q, p)$ under permutation of its arguments. Note that $\int dk T(k, p, q) \neq 0$. Figure 6a shows the contributions $T(k, s)$ of each octave of s to the total energy transfer $T(k)$ for the simulated inertial range. Recall that by construction the net transfer is zero, and figure 6a can more easily be interpreted as (the negative of) the contributions of the forcing and sub-grid viscosity. The measurement $T(k, s)$ for the inertial range gives us only limited information since the transfer at steady state is zero. More information can be extracted from $T(k, s)$ measurements in the DNS databases. Figure 6b shows that relatively local ($s < 4$) interactions dominate across most of the spectral space, while in contrast, figure 6c indicates that relatively nonlocal interactions become important at very large k . We will address this point with a more sensitive measurement, the fractional energy flux function, in following sections.

Recall that $T(k, p, q)$ in figure 5 is a smooth curve for each (p, q) with a pair of positive and negative peaks. The transfer sums $T(k, s)$ contain relatively more statistical noise because of the high degree of cancelation when the the raw interaction statistics are summed.

6. Analysis of the energy flux in the inertial range

The flux rate of energy across a scale k is the most basic measure of the energy transfer process. In the Kolmogorov theory of the universal equilibrium range it is the only link between the energetic and dissipative scales of motion. Contributions to the total flux from the various scale interactions can be written as

$$\Pi(k) = \sum_s \Pi(k, s), \quad (9a)$$

where

$$\Pi(k, s) = \int_k^\infty T(k', s) dk'. \quad (9b)$$

In the classical Kolmogorov inertial range, where energy injection is absent and dissipation is negligible, energy conservation implies that the energy flux across the spectrum is uniform. Note that this is a limiting situation as $Re \rightarrow \infty$. In such an ‘ideal’ inertial range, all of the dissipation occurs in the inertial range, but that *finite* dissipation is spread over an *infinite* range of scales so that the dissipation within any finite range of scales is zero.

Figure 7 displays the resolved energy flux and the contributions $\Pi(k, s)$ of the various scale disparities for the LES. While the Kolmogorov theory implies a uniform energy flux in the inertial range, the computed energy flux is not uniform because it includes only the numerically resolved-scales, and omits the flux due to the subgrid-eddy viscosity and forcing. When these are included, the flux is uniform by construction.

Figure 8 indicates that the fractional LES energy flux $\Pi(k, s)/\Pi(k)$ is dominated by local interactions (small scale disparity s) for all scales k . This closely resembles the classical picture of the energy transfer process described in detail by Tennekes and Lumley²⁰. Moreover, the dependence upon the scale disparity parameter is the same for all inertial range scales, that is beyond the forced scales the normalized individual energy flux contributions $\Pi(k, s)/\Pi(k)$ are essentially independent of k as would be expected in a scale-similar inertial range. In other words, $\Pi(k, s)/\Pi(k) \sim f(s)$. A less pronounced collapse can be seen for the high Reynolds number DNS where a decade of inertial range exists (figure 9). Note that the contributions for all s are of the same sign; there is no further cancellation in the sum over s (see figure 7).

7. Heisenberg and Obukhov energy transfer models in the inertial range

The detailed conservation property of $T(k, p, q)$ allows the energy flux through scale k to be divided into two parts:

$$\Pi(k) = \Pi^s(k) + \Pi^e(k) \quad (10)$$

where

$$\Pi^s(k) = \int_k^\infty dk' \int_0^k dp \int_0^k dq T(k', p, q), \quad (11a)$$

and

$$\Pi^e(k) = - \int_0^k dk' \int_k^\infty dp \int_k^\infty dq T(k', p, q). \quad (11b)$$

There are two types of non-local contributions to the energy flux resulting from distinct physical mechanisms: (1) when one of the wavenumbers [say p] in $\Pi^s(k)$ is very low while the other is $q \approx k$, $\Pi^s(k)$ is closely related to the classical energy transfer closure model of Obukhov²³ (see page 215 in Ref. 4) in which the strain due to the large scales causes local

energy transfer among the small scales, (2) when $p, q \gg k'$, $\Pi^e(k)$ is closely related to the classical eddy viscosity closure model of Heisenberg²⁴ (see page 217 in Ref. 4) in which the process of energy transfer from large to small eddies is qualitatively similar to the conversion of mechanical energy in a fluid into thermal energy via the kinematic viscosity. This forms the basis for the eddy viscosity model.

The dependence of the Heisenberg and Obukhov energy transfer models on s in the inertial range can easily be found. The Heisenberg energy transfer function is

$$\Pi^e(k) = \gamma_1 \int_k^\infty k'^{-3/2} [E(k')]^{1/2} dk' \int_0^k 2k''^2 E(k'') dk'',$$

while the Obukhov energy transfer function is

$$\Pi^s(k) = \gamma_2 \int_k^\infty E(k') dk' [\int_0^k k''^2 2E(k'') dk'']^{1/2},$$

where γ_1 and γ_2 are constants³. It is easy to show that

$$\Pi^e(k) \sim \int_{k'=k}^\infty d(k'^{-4/3}) \int_0^{k'=k} d(k''^{4/3})$$

and

$$\Pi^s(k) \sim \int_{k'=k}^\infty d(k'^{-2/3}) \int_0^{k'=k} d(k''^{2/3})$$

in an $E(k) \sim k^{-5/3}$ inertial range. When s is large, the three wavenumbers in a triad effectively reduce to two scales. As a result,

$$\Pi^e(k, s) / \Pi^e(k) \sim s^{-4/3},$$

and

$$\Pi^s(k, s) / \Pi^s(k) \sim s^{-2/3}$$

where $s = k'/k''$. While dimensional analysis can not be used to find the correct s dependence, the models can be compared to numerical simulations, and figure 8 indicates that the simulation data supports the $s^{-4/3}$ scaling of Heisenberg.

We calculate the contributions $\Pi^e(k, s)$ and $\Pi^s(k, s)$ of the various scale interactions, by partial summation of (10) and (11) over p and q in the same manner as before. The local interactions are shown in figures 10a and 10b to be more important than the nonlocal ones for both terms in (10) in agreement with the classical notion of an inertial subrange and with the $T(k, s)$ measurements above.

If we take the results at $k \sim 20$ to be representative (free from end effects) of the uniform flux, we can see some difference in the behaviors of $\Pi^s(k, s)$ and $\Pi^e(k, s)$. Π^s appears to decrease monotonically as s increases, while Π^e appears to grow with s up to about $2 < s < 4$,

and then to decrease at higher s . While the straining and eddy-viscosity interactions are of similar magnitude at this wavenumber, the straining interactions appear to dominate at high wavenumber. Indeed, these straining interactions are the source of the cusp in the spectral eddy viscosity in Kraichnan's formulation¹⁵. However, we must stress that the dominance of the straining interactions at high k is an artifact of the sharp spectral-cutoff that is used analytically in the renormalization group theory²⁵⁻²⁶ and numerically in our present measurements. Indeed, one would expect that the relative physical contributions of the eddy-viscosity and straining interactions in an inertial range would be invariant with k , as we found for the disparity contributions (see figure 8). The corresponding measurements for the high Reynolds number DNS are presented in figure 11.

8. Transfer estimates of Tennekes and Lumley

Tennekes and Lumley²⁰ (hereafter TL) estimated the energy transfer from the characteristic strain rates of different scales. In contrast to the models of Heisenberg and Obukhov, this model estimates separately the input and output of energy at a given k .

The rate of energy transfer into eddies of scale k is modelled by the production term $S_{ij}(q)\tau_{ij}(k)$, where τ is the Reynolds stress at scale k and $S(q) = (q^3 E(q))^{1/2}$ is the strain rate of eddies of scale q . Note that non-zero production requires that τ_{ij} be anisotropic.

The fractional contribution of scale q ($q < k$) to the total strain rate acting on scale k , and to the energy transfer rate into scale k , is then

$$\sim \frac{1}{S}(q^3 E(q))^{1/2}$$

where S is the total strain rate for all scales $q < k$.

The fractional distribution of the energy flux out of scale k can be estimated in the same manner. Again, let S be the combined strain rate of all eddies with wavenumbers below k , the time scale of the applied strain is of order $1/S$. TL utilized the concept of the return to isotropy and argued that the level of anisotropy of $\tau_{ij}(k)$ produced by the strain of larger scales depends on the time scale at k for return to isotropy $1/S(k) = (k^3 E(k))^{-1/2}$ relative to the time scale S^{-1} of the straining motion. Note that because smaller eddies have larger strain rates, small eddies return to isotropy rapidly.

The degree of anisotropy is assumed to be simply proportional to $S/S(k)$, and the energy transfer from all large eddies to an eddy of wavenumber k is approximately

$$\frac{S^2}{S(k)} k E(k).$$

Based on the analysis above, the fractional distribution over scales $q < k$ of the flux into scale k in an inertial range is proportional to

$$\sim q^{3/2} E(q)^{1/2} \sim q^{2/3} \sim s^{-2/3},$$

and the fractional distribution over $k > q$ of the flux out of q is proportional to

$$\sim k^{-1/2} E(k)^{1/2} \sim k^{-4/3} \sim s^{-4/3}.$$

Note that the input scales like the Obukhov model while the output scales like the Heisenberg model.

We have compared the measured transfers with the model of TL by breaking the net transfer (8b) into its separate input and output components, depending on their sign:

$$T^+(k, s) = \sum_{p, q | s} T(k, p, q) |_{T > 0} \quad (12b)$$

$$T^-(k, s) = \sum_{p, q | s} T(k, p, q) |_{T < 0} \quad (12b)$$

We observe in figure 12 that the input and output curves collapse for the various k as expected in a scale-similar inertial range and roughly follow the $-2/3$ and $-4/3$ powerlaws respectively, as predicted by TL. Similar results are obtained for the high Reynolds number DNS (figure 13) but the agreement with TL is not as clear.

9. Self-similarity of the energy transfer in the inertial range

We found in Sec. 6 that the fractional contributions to the energy flux are essentially independent of k as would be expected in a scale-similar inertial range. This strongly suggests that the transfer process is self-similar but it is important to confirm this directly.

Kraichnan⁹ pointed out that similarity within a Kolmogorov $k^{-5/3}$ inertial range implies the scaling

$$T(k, p, q) = a^3 T(ak, ap, aq) \quad (13)$$

if all six wave-numbers are in the inertial range. If we take $a = q^{-1}$, (13) reduces to

$$T(k, p, q) = q^{-3} T(k/q, p/q, 1) = q^{-3} F(k/q, p/q), \quad (14)$$

and the number of dependent variables is reduced from three to two. In figure 14 we have plotted $T(k, p, q)$ against k/q for several representative values of p/q . While there is a

good collapse of the curves for the various bands, a failure of self-similarity is observed for interactions involving bands near the spectral boundaries of the computation.

The transfer function

$$T(k, p) = \sum_q T(k, p, q) \quad (15)$$

gives the transfer of energy into k resulting from all interactions involving band p . Analogous to (13), the self-similar scaling law for $T(k, p)$ in the inertial range is

$$T(k, p) = a^2 T(ak, ap). \quad (16)$$

We can further reduce (16) to

$$T(k, p) = p^{-2} T(k/p, 1) = p^{-2} H(k/p). \quad (17)$$

This self-similar law is also well satisfied except for p near the computational boundaries, as shown in figure 15.

In both figures 14 and 15, self-similar profiles can be found by averaging over the collapsed curves, and such averaged $T(k, p)$ values have been marked in figure 15.

Note that the question of the locality of dominant interactions can be answered in terms of figure 15. When s is large, the three wavenumbers in a triad effectively reduce to two scales. $T(k, p)$ provides a direct measurement of the locality since self-similarity further reduces the variables to one, implying an equivalence between s and the ratios k/p or p/k when they are large. While an interaction range of $s = 50$, as seen in figure 15, may seem rather “non-local”, the basic question really is whether the interaction range is large enough to contain both the energetic and dissipation scales at large Reynolds number. The rapid $s^{-4/3}$ decay, shown in figure 16, would seem to rule that out.

From the detailed balance and figure 15, one expects that $T(k, p)$ is antisymmetric at large s , that is $H(s) = -H(1/s)$. Figure 16 shows that this is indeed the case. The deviation at very large s is due to numerical error.

10. The ‘ideal’ Kolmogorov energy transfer and inertial range

The failure of self-similarity near the computational boundaries is a numerical artifact of the forcing and eddy viscosity used in the LES. This suggests that the numerical artifacts can be eliminated, or at least reduced, by using the self-similar scaling to filter the raw data. Essentially, the data redundancy implied by the scaling law’s reduction of three variables to two allows us to reduce the error associated with end-effects of the computational domain. To obtain the corrected data, we have simply removed the curves associated with bands near the boundaries that did not collapse and averaged the remaining ones. Such an operation

reduces the data to a single curve that can be viewed as the ‘ideal’ one, that is, the one that would be obtained in an infinitely long inertial range. As a result, we are able to *construct* the ‘ideal’ energy transfer function $T(k)$ in an infinite inertial range, by integrating the self-similar $T(k, p)$ over a finite range of p .

A suitable analogy for such an infinitely long inertial range is an infinitely long ‘pipe’ without leaks. To illustrate the interaction of scales, we ‘cut’ a finite section from this ‘pipe’ and view its inflow and outflow. The finite section of pipe corresponds to the finite range of the integral over p mentioned above. The “ideal” $T(k)$ constructed from simulations of size 64^3 , 128^3 and 256^3 are shown in figure 17. The negative and positive peaks correspond to inflow and outflow. Since the flow is statistically steady and $\int dkT(k) = 0$, we have shifted the peaks so that the three mesh sizes overlap. Because the ‘ideal’ pipe does not leak, its length is not important. This is a direct visualization of the Kolmogorov energy transfer process in a finite section of the ‘ideal’ inertial range, and the ‘ideal’ inflow and outflow profiles are quite different from actual measured transfer spectra (figure 4a). Indeed, the ‘pipe’ concept is suggested by the long range of scales in figure 4a in which the net transfer is very small.

11. A determination of the Kolmogorov constant

Experiments at high Reynolds number give values of the Kolmogorov constant in the range of $C_k \sim 1.5$ (Monin and Yaglom⁴), but values determined directly from spectra in numerical simulations are usually around 2. (Vincent and Meneguzzi²⁷, Sanada¹⁹, Chasnov¹⁴).

From inspection of the energy spectrum of the high Reynolds number DNS at $R_\lambda \sim 200$ (figure 2), we would estimate the Kolmogorov constant to be about 2.3. Preliminary work of Shiyi Chen (private communication, 1993) suggested that a more realistic Kolmogorov constant may be estimated from DNS by experimenting with the choices of Reynolds number and resolution. For the inertial range LES data, the dissipation rate estimated from the maximum resolved energy flux is .45 (figure 7), giving a value of the Kolmogorov constant of 1.7. (Recall that the energy spectrum was held constant at $E(k) = k^{-5/3}$ so that $C_k \epsilon^{2/3} = 1$).

We can also measure the energy flux as the integral of the inflow or outflow of the ‘ideal’ pipe (figure 17). This gives a flux value of about .64 and a corresponding Kolmogorov constant $C_k \sim 1.5$. This ‘ideal’ energy dissipation rate, evaluated using the self-similar law, has hopefully eliminated the computational artifacts resulting from the limited computational domain.

12. Analysis of the energy flux in the far-dissipation range

In figure 18a we display the fractional contributions to the energy flux across different scales k for the low-Reynolds number forced DNS. The curves for the various k do not collapse, in contrast with the results in the inertial range. Instead, the scale disparity increases with k . Analytical theories generally assume that the dynamics of the very small scales in these ranges is controlled by interactions with the much larger Kolmogorov scales at which the highest strain rates occur²⁸. To test this assumption, we replot the data against $k_d s/k$ in figure 18b. The agreement with the analytical assumption is quite good (note that the theory actually over predicts the rescaling). This suggests that $\Pi(k, s)/\Pi(k) \sim f(\frac{sk_d}{k})$ and the energy transfer is dominated by increasingly non-local interactions. A more detailed analysis²⁹ has appeared in the Proceedings of 1992 CTR Summer Program. Domaradzki³⁰ proposed an empirical model for the far-dissipation range based on a scaling law³¹ that collapses measured $T(k, p, q)$. The model predicts the exponential decay of the energy spectrum with wavenumber.

13. Conclusions

The basic energy transfer function $T(k, p, q)$, which measures the energy flow produced by the interaction of sharply truncated Fourier bands, is the starting point for the analysis of the transfer of energy across the scales in a turbulent flow. At issue is the appropriate choice of a statistical quantity to indicate the nature of energy transfer across the spectrum, and particularly its dependence on the relative scales involved in the nonlinear interactions. Previous authors have interpreted the scaling of the interaction directly from the raw interaction measurements⁶⁻⁸. Our results support Kraichnan's⁹ view that $T(k, p, q)$ is the fundamental building block in the energy transfer process but not the quantity one should use to determine whether the dominant nonlinear interactions are local or nonlocal. For a given scale k , we have summed the raw interaction statistics such that physical quantities, for example the energy flux, contain only *one* parameter, s , that indicates the scale disparity of the interaction and we have determined how these quantities depend on s . We found that the net flux in the inertial range results primarily from relatively local interactions and that contributions decrease as $s^{-4/3}$ for large disparity.

We have compared the measured s dependence of the transfer process (LES dataset) with several classical energy transfer models, specifically those advanced by Heisenberg²⁴, Obukov²³, and Tennekes and Lumley²⁰. These models are built on different physical as-

sumptions and their validity can not be determined by dimensional analysis.

The measured energy transfer is reasonably self-similar for wavenumbers in the inertial range. Artifacts of the finite computational domain, the LES models, can be identified and to some extent eliminated by constructing an 'ideal' energy transfer function. The energy flux, corrected for the loss due to the finite computation domain, was used to calculate the Kolmogorov constant 1.5, in excellent agreement with experiments⁴.

We have presented a comparison of the compensated energy spectra for a high-Reynolds number decaying DNS and a low-Reynolds number forced DNS. The far-dissipation energy spectrum is found to be $\sim \exp(-\alpha k\eta)$ with the range of α is $4.9 \sim 5.1$, in agreement with previous investigations¹⁷⁻¹⁹. The energy transfer process in the far-dissipation range is found to be dominated by non-local interactions with a scale disparity that increases with increasing wavenumber. This is consistent with classical theories that assume that scales smaller than the Kolmogorov scale are slaved to it.

It should be noted that studies of the type presented here are limited to the question of the statistical importance of interactions between various scales, and are not capable of addressing questions of physical structure or mechanisms.

Acknowledgments

The author gratefully acknowledges stimulating discussions with Dr. R.S. Rogallo and Dr. R.H. Kraichnan. The author is indebted to Dr. R.S. Rogallo for his assistance with the computations, and to Dr. J.R. Chasnov and Dr. G. Erlebacher for their comments on a draft of the manuscript. Time on the Intel Hypercube was furnished by the NAS division at NASA Ames Research Center. He thanks Professor P. Moin and Professor W. C. Reynolds for their support.

References

1. *Proc. Roy. Soc. London*, **434**, 1-240 (1991)
2. A. N. Kolmogorov, "The local structure of turbulence in incompressible viscous fluid for very large Reynolds number". *Dokl. Akad. Nauk SSSR*, **30**, 301 (1941).
3. G.K. Batchelor, *The theory of homogeneous turbulence* (Cambridge Univ. Press, Cambridge, UK, 1953)
4. A.S. Monin and A.M. Yaglom, *Statistical Fluid Mechanics* (MIT Press, 1975), Vol. 2.
5. D. Chapman, "Computational aerodynamics development and outlook". *AIAA J.*, **17**, 1293 (1979)
6. J. A. Domaradzki and R.S. Rogallo, "Local energy transfer and nonlocal interactions in homogeneous, isotropic turbulence", *Phys. Fluids A*, **2**, 413 (1990).
7. P.K. Yeung and J. G. Brasseur, "The response of isotropic turbulence to isotropic and anisotropic forcing at large scales," *Phys. Fluids A*, **3**, 884 (1991).
8. K. Ohkitani and S. Kida, "Triad interactions in a forced turbulence", *Phys. Fluids A*, **4**, 794 (1992).
9. R. H. Kraichnan, "Inertial-range transfer in two- and three- dimensional turbulence", *J. Fluid Mech.*, **47**, 525 (1971).
10. J. R. Chasnov, "Similarity states of passive scalar transport in isotropic turbulence", *Phys. Fluids A*, to appear.
11. R.S. Rogallo and P. Moin, "Numerical simulation of turbulent flows", *Ann. Rev. Fluid Mech.*, **16**, 99 (1984).
12. R.H. Kraichnan, in "Theoretical approaches to turbulence", edited by D. L. Dwoyer, M.Y. Hussaini and R.G. Voight (Springer-Verlag, NY 1985).
13. Z.-S. She and E. Jackson, "A constrained Euler system for Navier-Stokes turbulence", *Phys. Rev. Lett.* (1993).
14. J. R. Chasnov, "Simulation of the Kolmogorov inertial subrange using an improved subgrid model" *Phys. Fluids A*, **11**, 945 (1991).
15. R.H. Kraichnan, "Eddy viscosity in two and three dimensions", *J. Atmos. Sci.*, **33**, 1521 (1976).
16. F. Anselmet, Y. Gagne, E.J. Hopfinger and R. A. Antonia, "High-order velocity structure functions in turbulent shear flows", *J. Fluid Mech.*, **140**, 63 (1984).
17. R.M. Kerr, "Velocity, scalar, and transfer spectra in numerical turbulence", *J. Fluid Mech.*, **211**, 309 (1990)
18. T. Sanada, "Cluster statistics of homogeneous fluid turbulence", *Phys. Rev. A*, **44**, 6480 (1991).
19. S. Kida and Y. Murakami, "Kolmogorov similarity in freely decaying turbulence",

Phys. Fluids, **30**, 2030 (1987)

20. H. Tennekes and J.L. Lumley, *A First course in turbulence* (MIT press, Cambridge, MA, 1972)

21. F. Waleffe, "The nature of triad interactions in homogeneous turbulence", *Phys. Fluids A*, **4**, 350 (1992)

22. M. Lesieur, *Turbulence in Fluids* (Martinus Nijhoff Publisher, 1990).

23. A.M. Obukhov, "Structure of the temperature field in turbulent flows", *Isv. Geogr. Geophys. Ser.*, **13**, 58, (1949).

24. W. Heisenberg, "Zur statistischen theorie der turbulenz", *Z. Physik*, **124**, 628, (1948).

25. Y. Zhou, G. Vahala, and M. Hossain, "Renormalization-group theory for the eddy viscosity in subgrid modeling" , *Phys. Rev. A*, **37**, 2590 (1988).

26. Y. Zhou, G. Vahala, and M. Hossain, "Renormalized eddy viscosity and Kolmogorov's constant in forced Navier-Stokes turbulence" , *Phys. Rev. A*, **40**, 5865 (1989).

27. A. Vincent and M. Meneguzzi, "The spatial structure and statistical properties of homogeneous turbulence", *J. Fluid Mech.* , **225**, 1 (1991).

28. G. K. Batchelor, "Small-scale variation of convected quantities like temperature in turbulent fluid", *J. Fluid Mech.*, **5**, 113 (1959).

29. S. Kida, R.H. Kraichnan, R.S. Rogallo, F. Waleffe, and Y. Zhou, in *Proc. of the Summer Program 1992*, Center for Turbulence Research, Stanford Univ. and NASA / AMES Research Center.

30. J.A. Domaradzki, "Nonlocal triad interactions and the dissipation range of isotropic turbulence", *Phys. Fluids A*, **4**, 2037 (1992)

31. J.A. Domaradzki, R.S. Rogallo, and A.A. Wray, "Interscale energy transfer in numerical simulated homogeneous turbulence", in *Proc. of the Summer Program 1990*, Center for Turbulence Research, Stanford Univ. and NASA / AMES Research Center.

flows	ν	ϵ	η	R_λ
LES	$\nu_t(k)$	0.65	—	∞
d256x4	0.02	1254	0.0089	~ 200
f256a	0.01	13.16	0.0166	~ 40
jc2f	$\nu_t(k)$	—	—	∞

Table 1. Main turbulence characteristics of the flow fields. For LES, ϵ is the energy flux found as the integral of the inflow or outflow of the 'ideal' pipe (figure 17). For the two DNS, ϵ is the actual viscous dissipation.

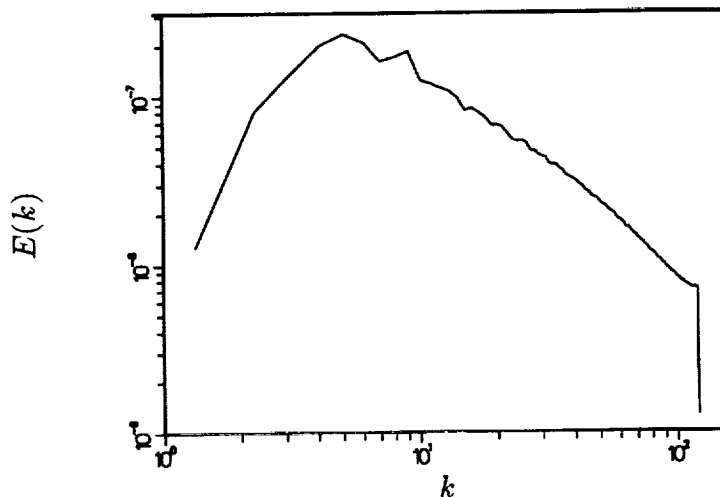


FIGURE 1. The energy spectrum for the decaying LES of the large-scale range.

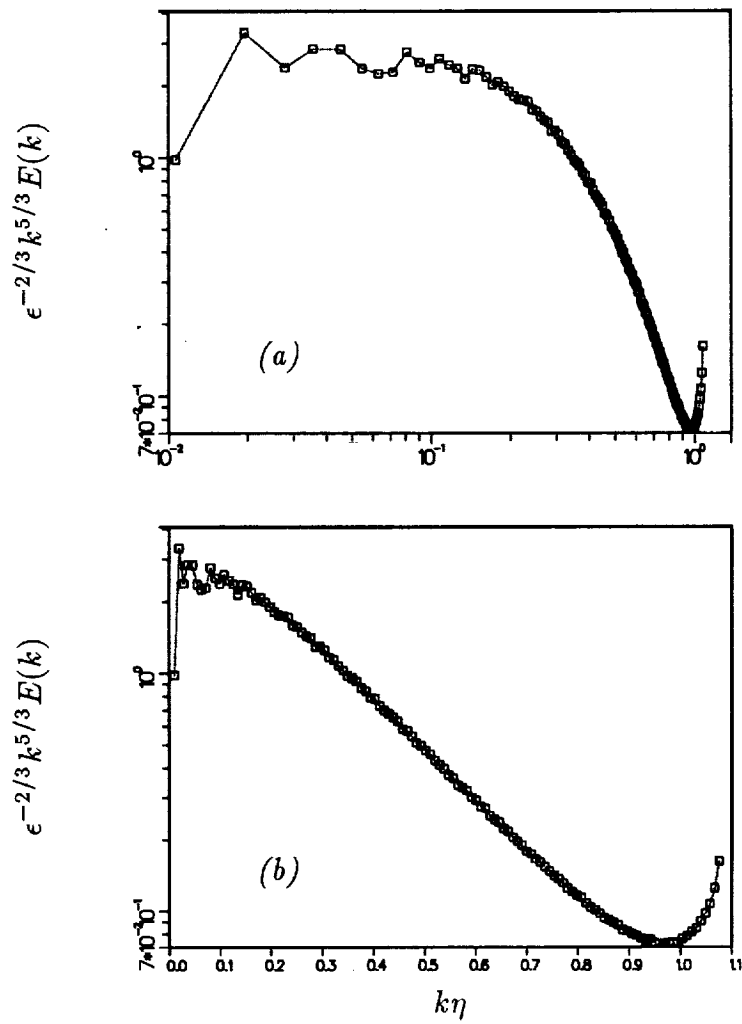


FIGURE 2. The compensated energy spectrum for the decaying DNS at $R_\lambda \sim 200$. (a) logarithmic plot: the spectrum below $k\eta = .1$ gives an estimate of the Kolmogorov constant. (b) linear plot: the central part decays with wavenumber as $\exp(-4.9k\eta)$.

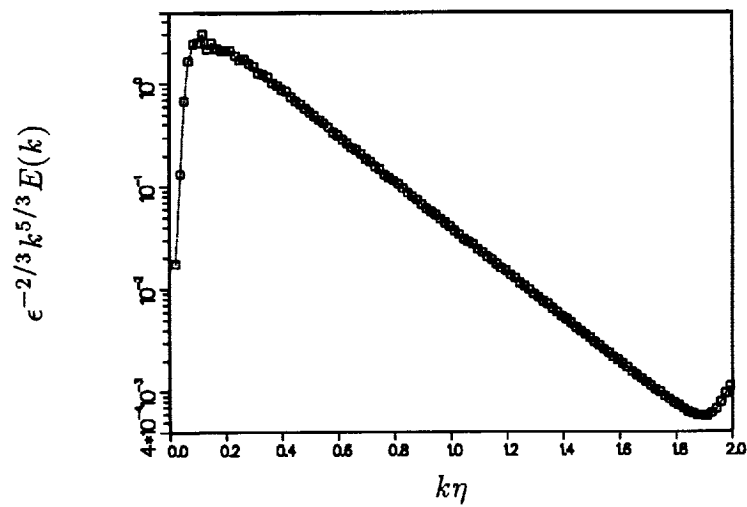


FIGURE 3. The compensated energy spectrum for the forced DNS at $R_\lambda \sim 40$. The central part decays with wavenumber as $\exp(-5.1k\eta)$.

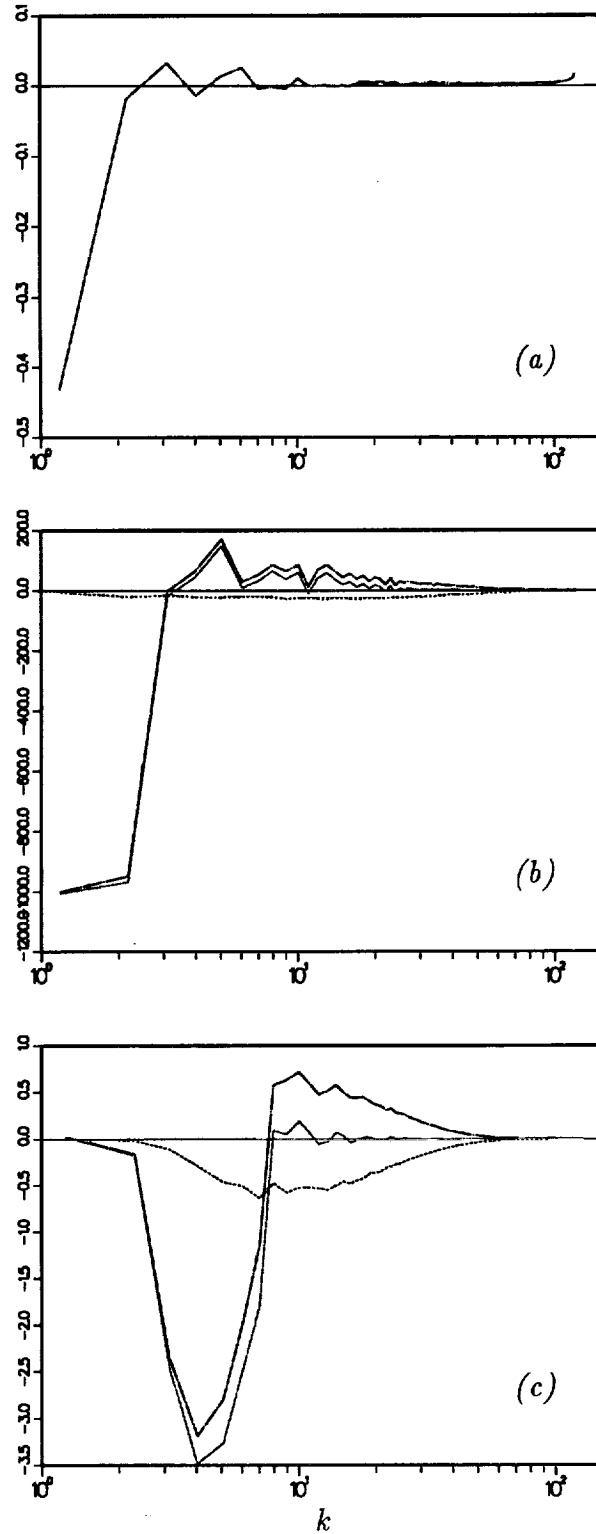


FIGURE 4. Energy budgets of the simulations: —, transfer $T(k)$; ----, dissipation $2\nu \int k^2 E(k) dk$; ·····, transfer - dissipation. (a) inertial-range LES at one instant. (b) decaying DNS at $R_\lambda \sim 200$: (c) forced DNS at $R_\lambda \sim 40$: There is an instantaneous equilibrium between transfer and dissipation for high k in the DNS.

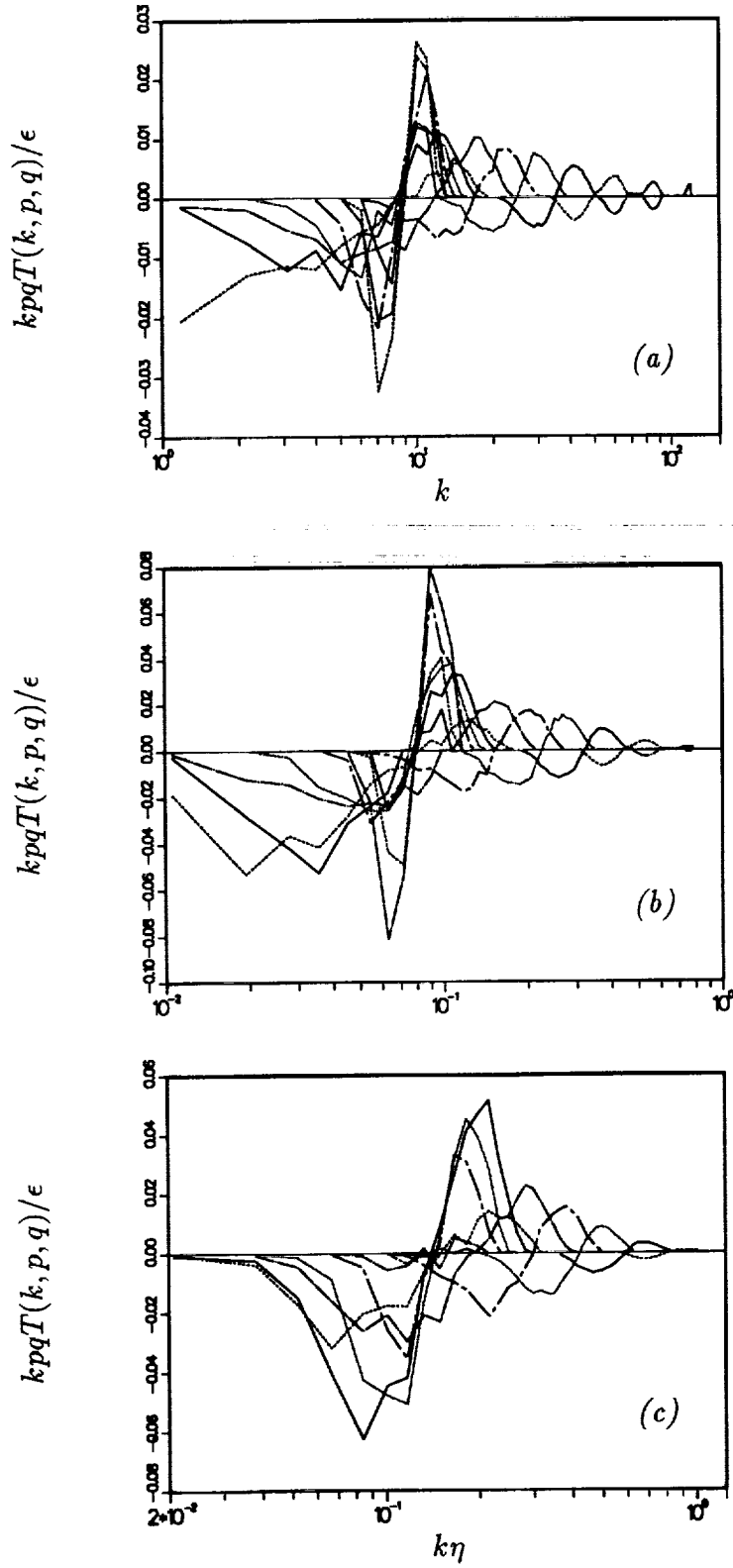


FIGURE 5. The interaction transfers $T(k, p, q)$ involving $2^{7/2} < p < 2^{8/2}$ and all q bands: (a) inertial-range LES; (b) decaying DNS at $R_\lambda \sim 200$; (c) forced DNS at $R_\lambda \sim 40$. The curves correspond, left to right, to increasing q .

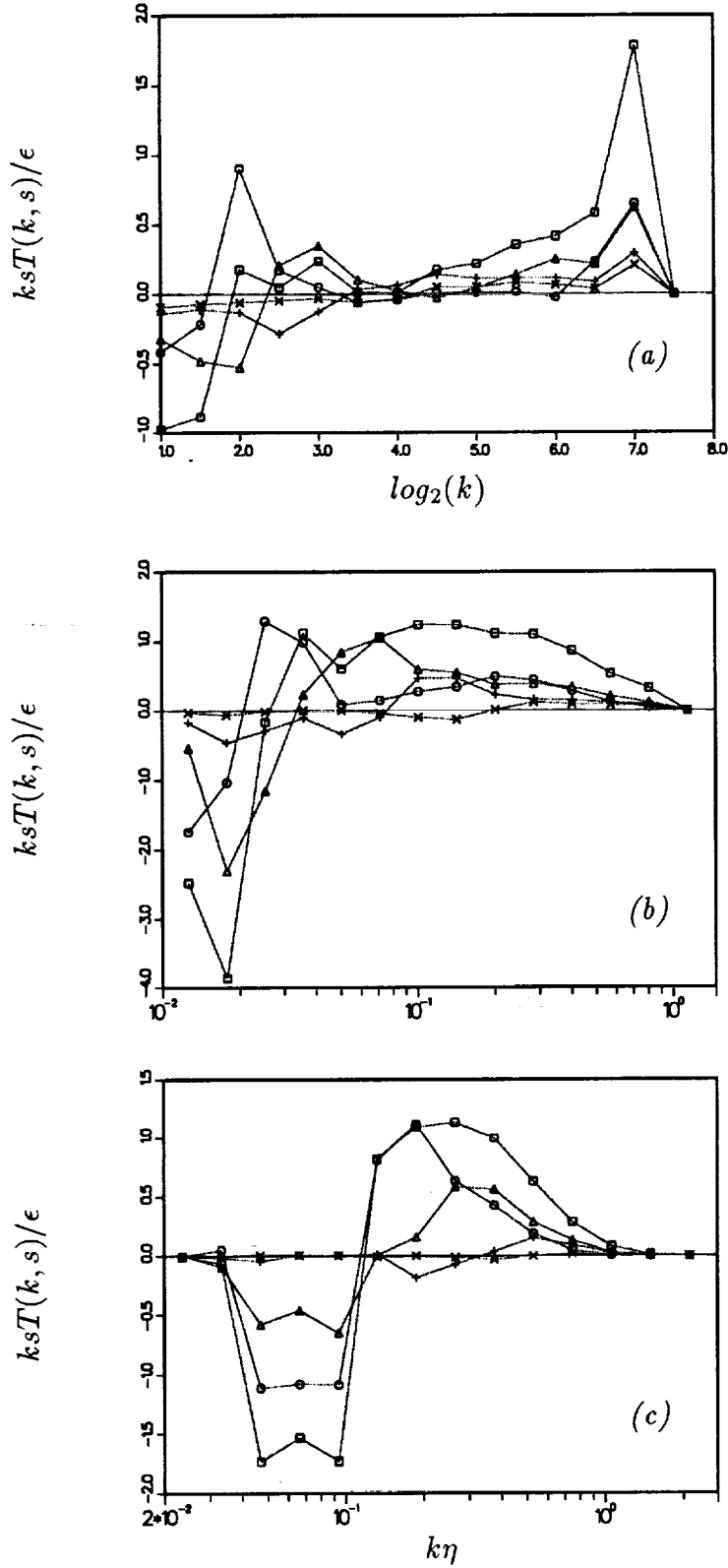


FIGURE 6. Contributions to the transfer spectrum by interactions of various disparities: \square , total $kT(k)/\epsilon$; \circ , $1 < s < 2$; \triangle , $2 < s < 4$; $+$, $4 < s < 8$; \times , $s > 8$. (a) inertial range LES; (b) decaying DNS at $R_\lambda \sim 200$ (c) forced DNS at $R_\lambda \sim 40$.

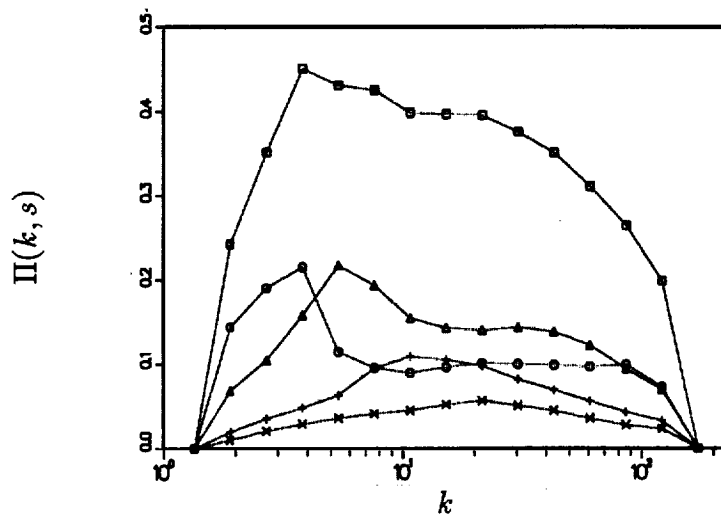


FIGURE 7. Contributions $\Pi(k, s)$ to energy flux in the inertial range LES. \square , total; \circ , $1 < s < 2$; \triangle , $2 < s < 4$; $+$, $4 < s < 8$; \times , $s > 8$.

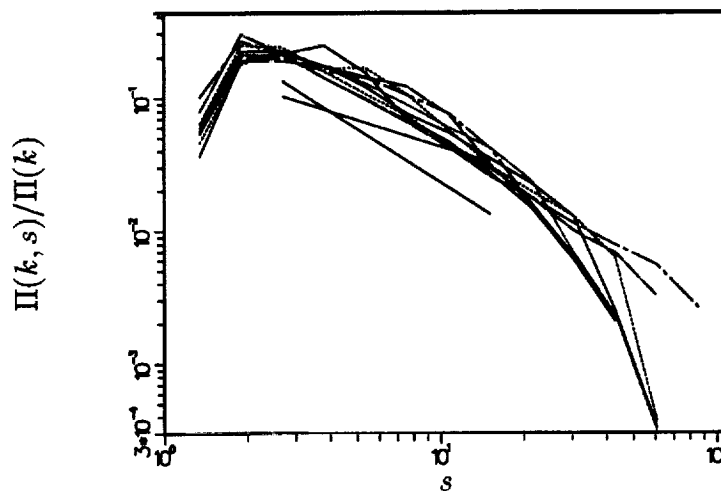


FIGURE 8. Fractional contribution $\Pi(k, s)/\Pi(k)$ to the energy flux in the inertial range LES. The various curves are for $k = 2^{n/2}$, $6 \leq n \leq 14$. The straight lines indicate $s^{-2/3}$ and $s^{-4/3}$ behaviors.

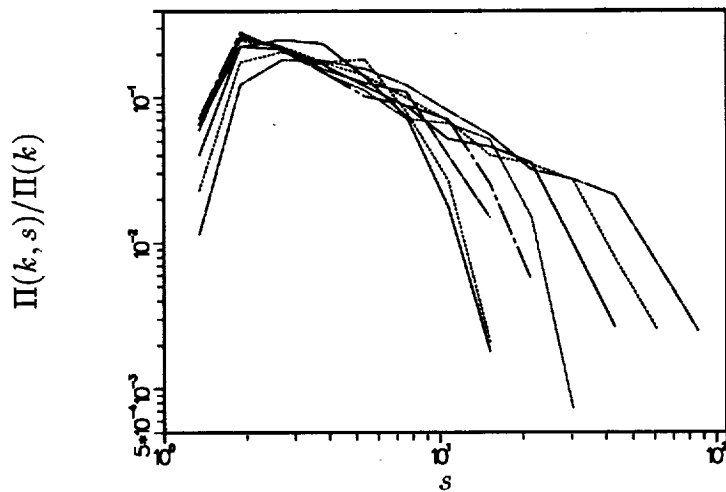


FIGURE 9. Fractional contribution $\Pi(k, s)/\Pi(k)$ to the energy flux for the decaying DNS at $R_\lambda \sim 200$. The dependence of energy flux upon the scale disparity of contributing interactions is illustrated. The various curves from left to right are for $k = 2^{n/2}, 6 \leq n \leq 14$.

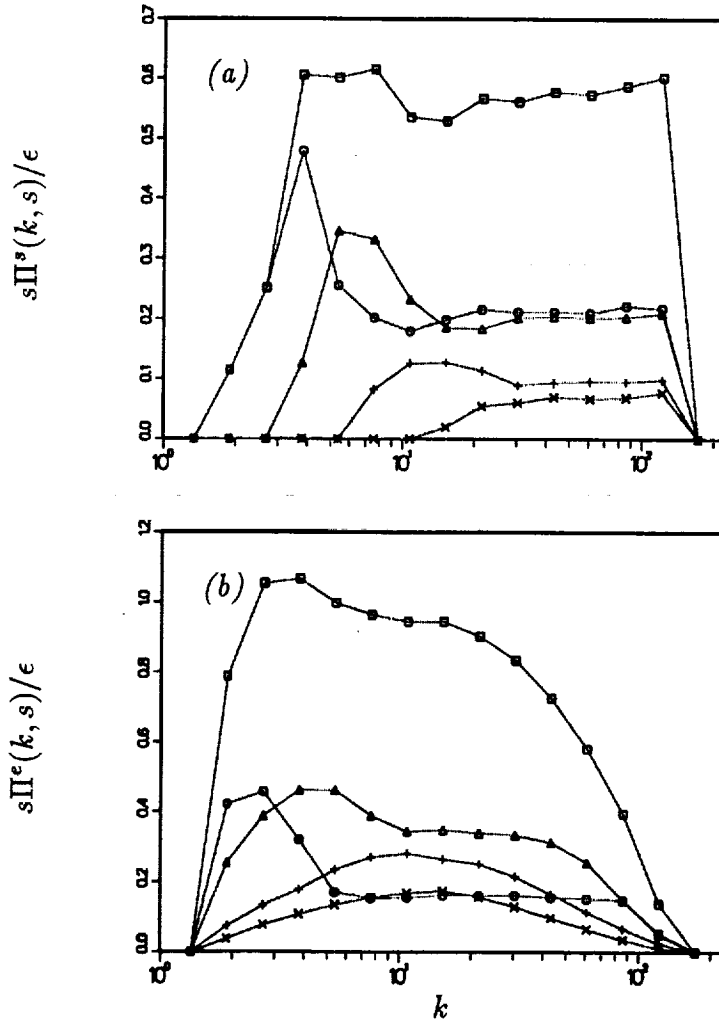


FIGURE 10. Contributions to the energy flux in the inertial range: \square , total $\Pi^s(k,s)/\epsilon$; \circ , $1 < s < 2$; \triangle , $2 < s < 4$; $+$, $4 < s < 8$; \times , $s > 8$. (a) Straining (Obhukov) interactions; (b) eddy-viscosity (Heisenberg) interactions.

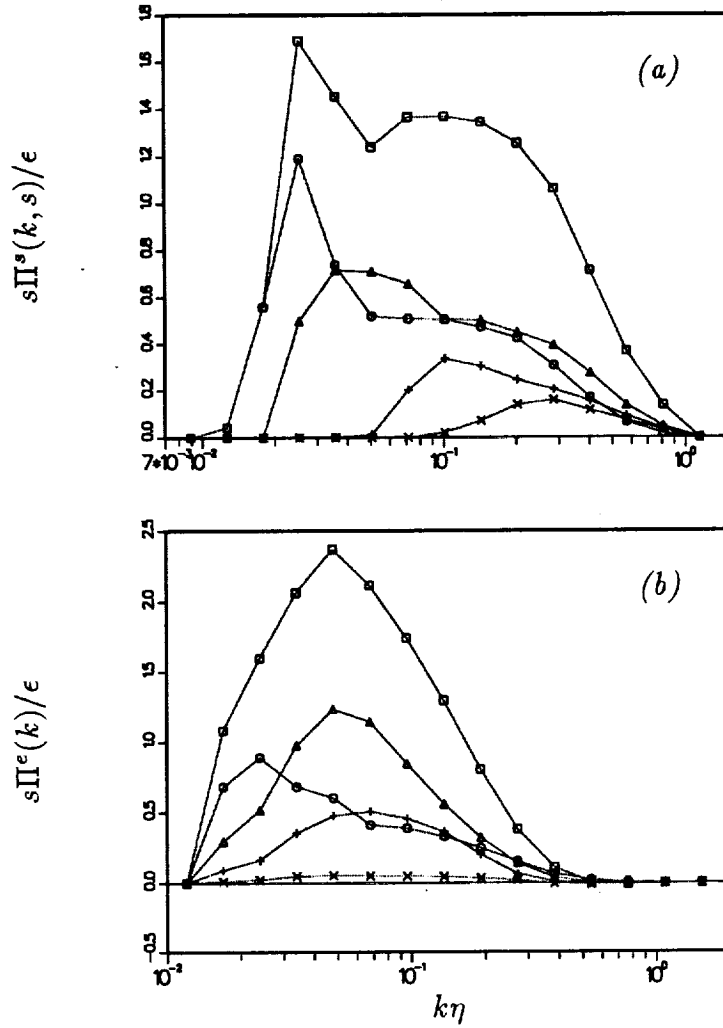


FIGURE 11. Contributions to the energy flux for the decaying DNS at $R_\lambda \sim 200$: \square , total $\Pi^s(k)/\epsilon$; \circ , $1 < s < 2$; \triangle , $2 < s < 4$; $+$, $4 < s < 8$; \times , $s > 8$. (a) Straining (Obhukov) interactions; (b) Eddy viscosity (Heisenberg) interactions. The straining interactions dominate at high $k\eta$ as predicted by Domaradzki³⁰.

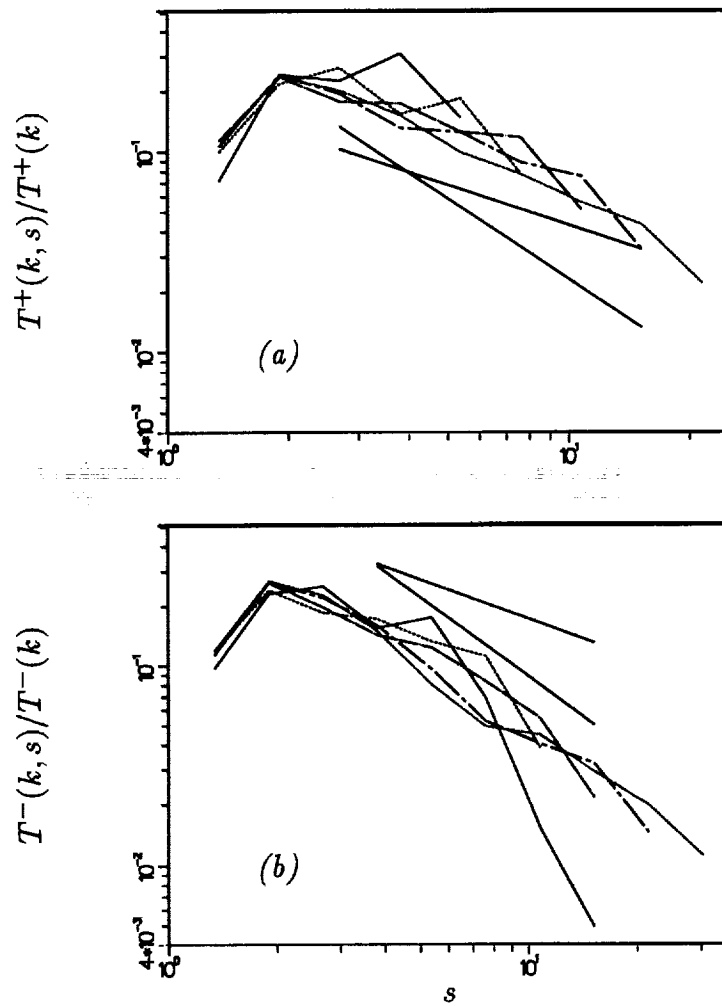


FIGURE 12. Fractional input and output distributions of the energy flux through scale k for the inertial range LES: (a) input; (b) output. The range of k is the same as in Figure 8. The straight lines indicate $s^{-2/3}$ and $s^{-4/3}$ behaviors.

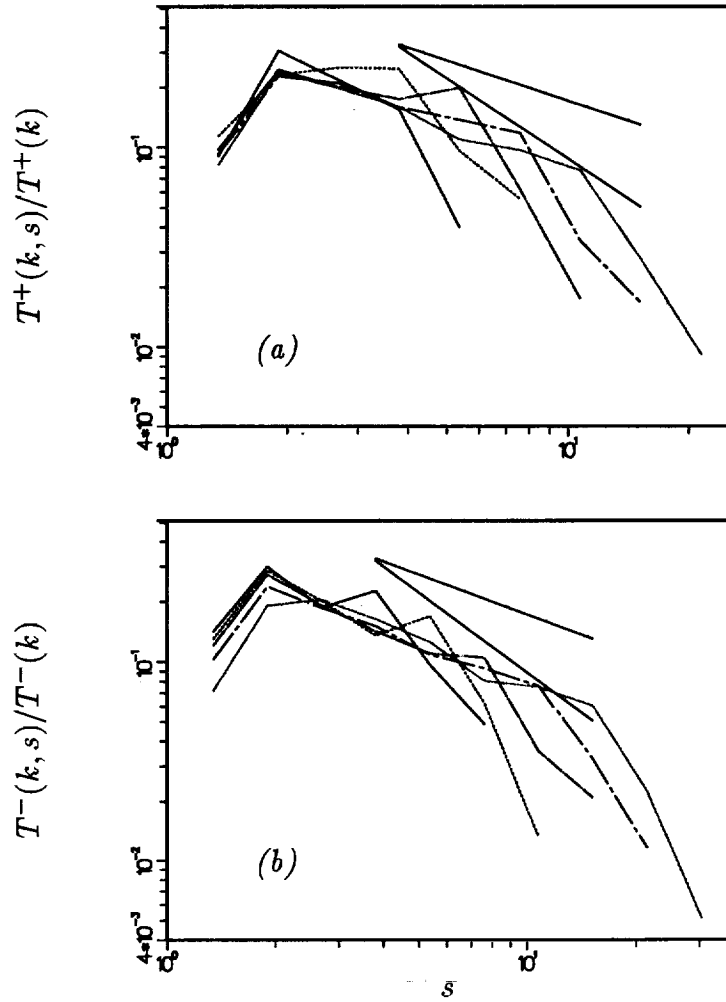


FIGURE 13. Fractional input and output distributions of the energy flux through scale k for the high Reynolds number DNS: (a) input; (b) output. The range of k is the same as in Figure 9. The straight lines indicate $s^{-2/3}$ and $s^{-4/3}$ behaviors.

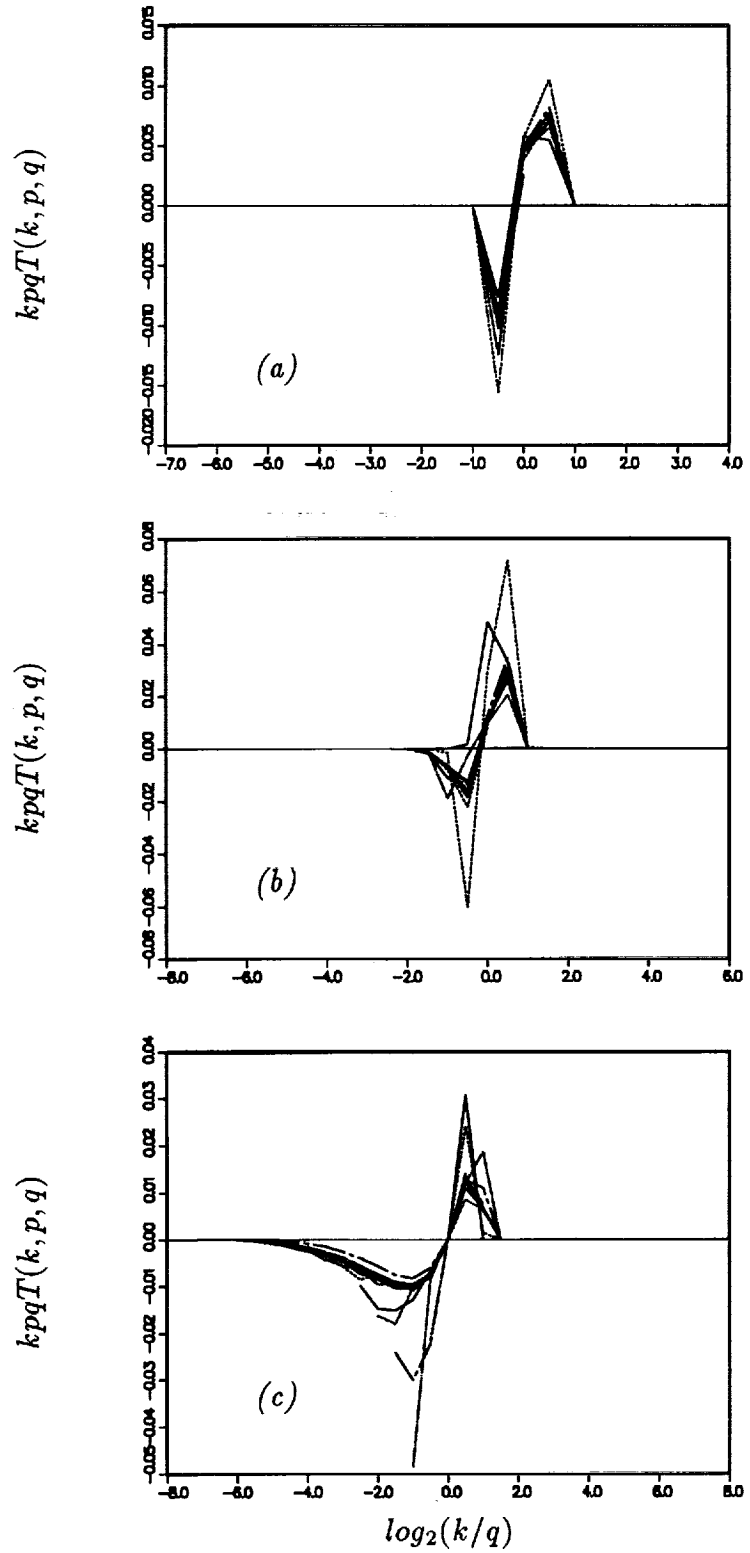


FIGURE 14. Direct verification of self-similarity (14) of the transfer $T(k, p, q)$ in the inertial range. (a) $p/q = 1/8$; (b) $p/q = 1/4$; (c) $p/q = 1$.

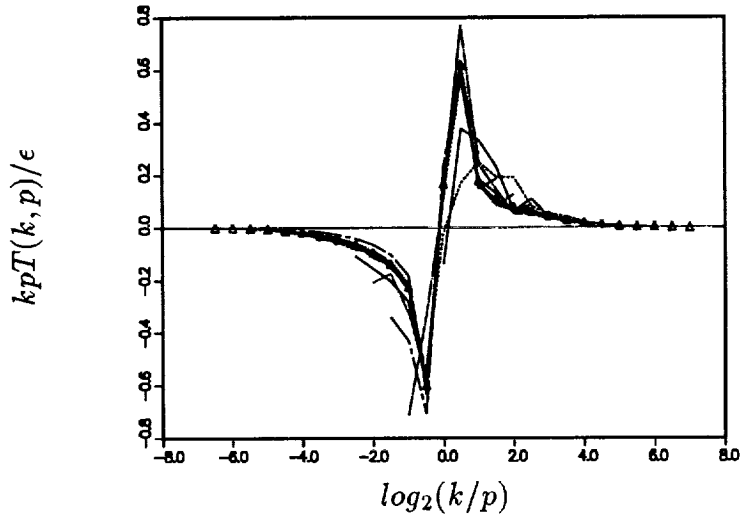


FIGURE 15. Self similarity of the transfer function $T(k, p)$ in an inertial range. The curves are for the various p bands of the inertial range LES. The points Δ are the average values of $H(k/p)$ used to represent the “ideal” inertial range.

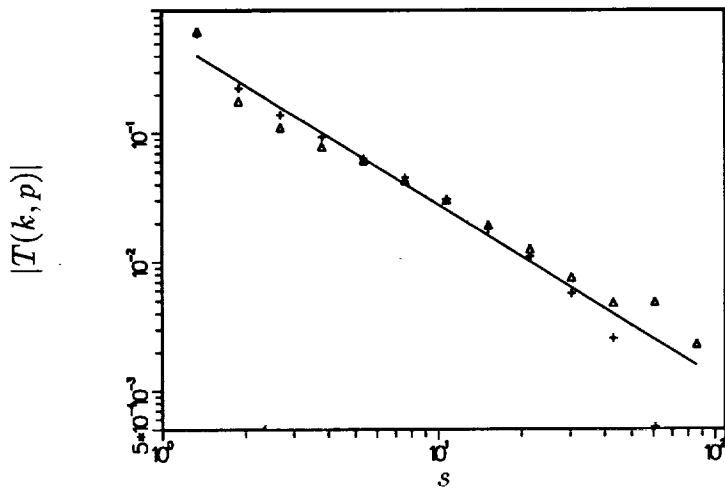


FIGURE 16. The self-similar transfer function $T(k, p)$: Δ , $s = k/p$; $+$, $s = p/k$. The line indicates a $s^{-4/3}$ behavior. The scatter at large s is due to numerical error.

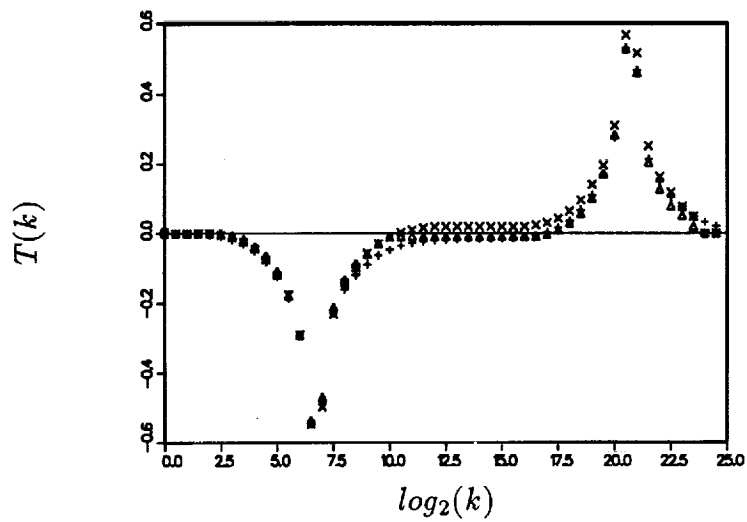


FIGURE 17. The 'ideal' self-similar transfer $T(k)$: \triangle , 64^3 mesh; $+$, 128^3 mesh; \times , 256^3 mesh.

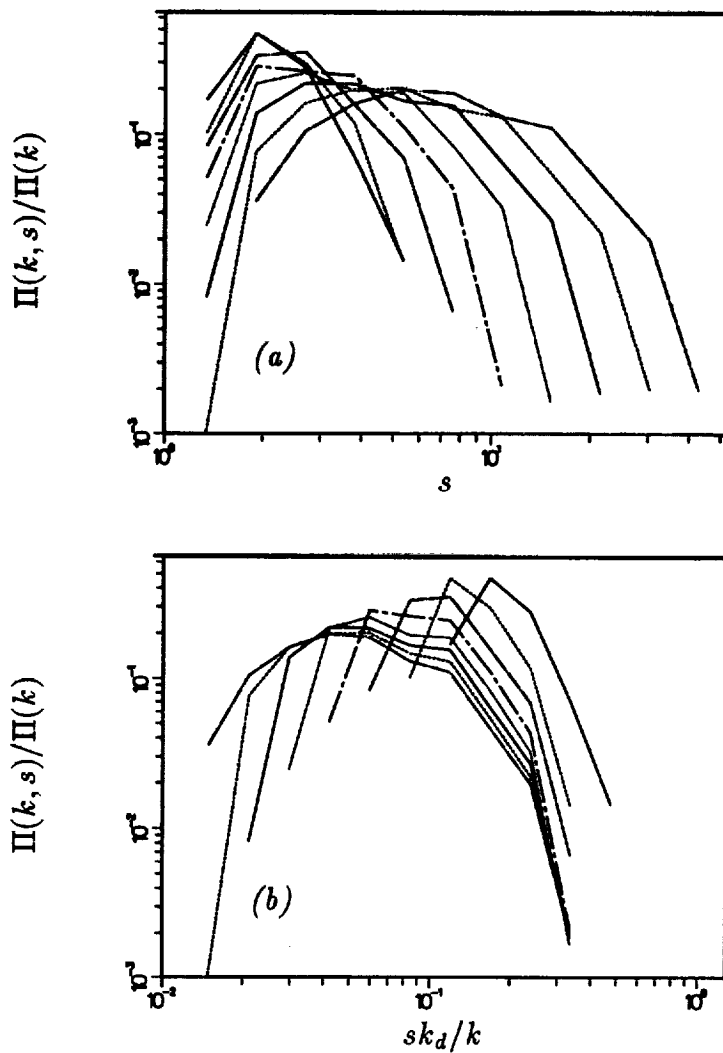
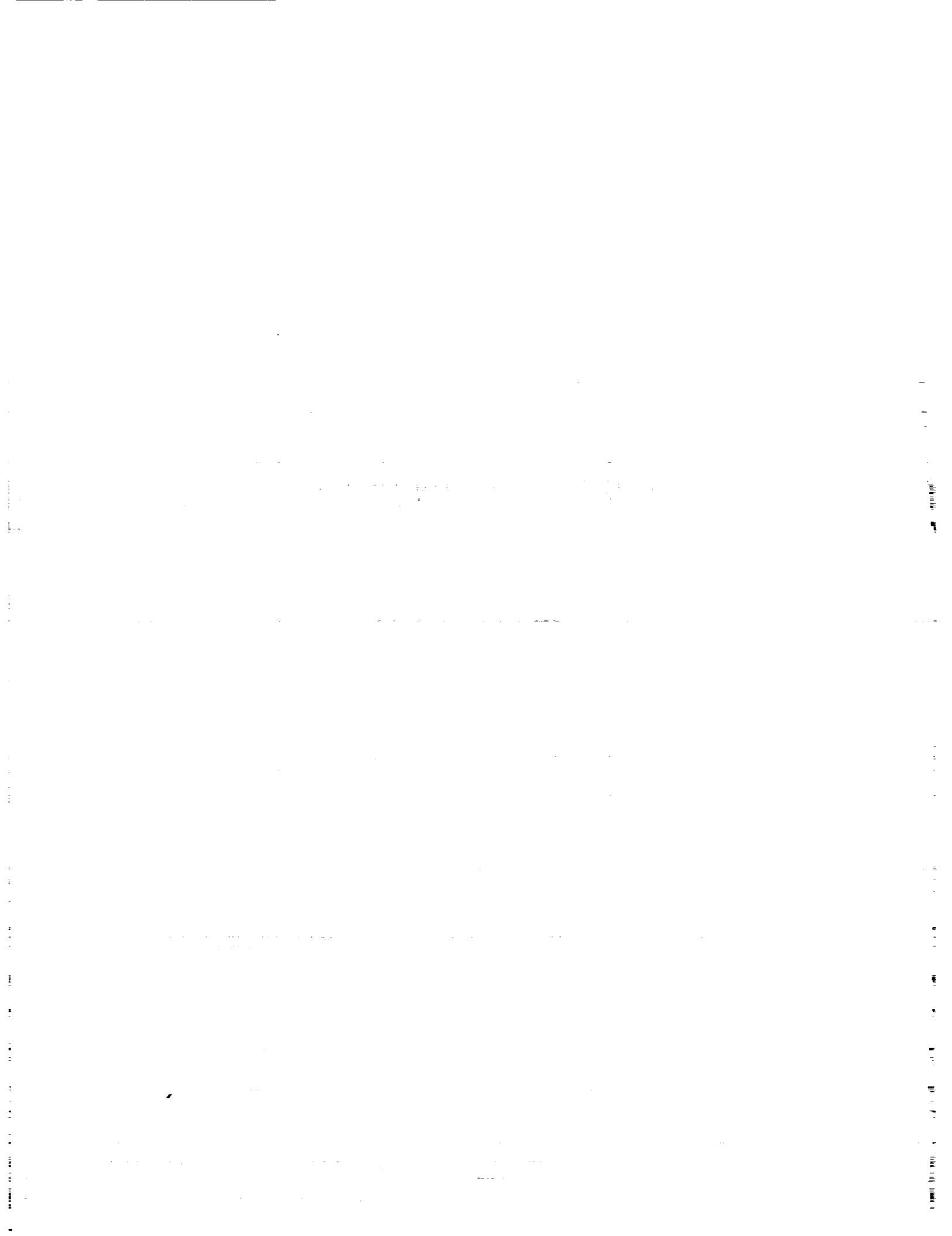


FIGURE 18. Fractional contribution $\Pi(k, s)/\Pi(k)$ to the energy flux in the dissipation-range DNS. (a) plotted against s , the curves are for k increasing left to right, (b) plotted against sk_d/k , the curves are for increasing k right to left.



REPORT DOCUMENTATION PAGE			Form Approved OMB No. 0704-0188	
Public reporting burden for this collection of information is estimated to average 1 hour per response, including the time for reviewing instructions, searching existing data sources, gathering and maintaining the data needed, and completing and reviewing the collection of information. Send comments regarding this burden estimate or any other aspect of this collection of information, including suggestions for reducing this burden, to Washington Headquarters Services, Directorate for Information Operations and Reports, 1215 Jefferson Davis Highway, Suite 1204, Arlington, VA 22202-4302, and to the Office of Management and Budget, Paperwork Reduction Project (0704-0188), Washington, DC 20503				
1. AGENCY USE ONLY (Leave blank)	2. REPORT DATE June 1993	3. REPORT TYPE AND DATES COVERED Contractor Report		
4. TITLE AND SUBTITLE INTERACTING SCALES AND ENERGY TRANSFER IN ISOTROPIC TURBULENCE		5. FUNDING NUMBERS NAS1-19480 WU 505-90-52-01		
6. AUTHOR(S) Ye Zhou				
7. PERFORMING ORGANIZATION NAME(S) AND ADDRESS(ES) Institute for Computer Applications in Science and Engineering Mail Stop 132C, NASA Langley Research Center Hampton, VA 23681-0001		8. PERFORMING ORGANIZATION REPORT NUMBER ICASE Report No. 93-28		
9. SPONSORING/MONITORING AGENCY NAME(S) AND ADDRESS(ES) National Aeronautics and Space Administration Langley Research Center Hampton, VA 23681-0001		10. SPONSORING/MONITORING AGENCY REPORT NUMBER ICASE Report No. 93-28 NASA CR-191477		
11. SUPPLEMENTARY NOTES Langley Technical Monitor: Michael F. Card Final Report		Submitted to the Physics of Fluids A		
12a. DISTRIBUTION/AVAILABILITY STATEMENT Unclassified - Unlimited Subject Category 34		12b. DISTRIBUTION CODE		
13. ABSTRACT (Maximum 200 words) <p>The dependence of the energy transfer process on the disparity of the interacting scales is investigated in the inertial and far-dissipation ranges of isotropic turbulence. The strategy for generating the simulated flow fields and the choice of a disparity parameter to characterize the scaling of the interactions is discussed. The inertial range is found to be dominated by relatively local interactions, in agreement with the Kolmogorov assumption. The far-dissipation is found to be dominated by relatively non-local interactions, supporting the classical notion that the far-dissipation range is slaved to the Kolmogorov scales. The measured energy transfer is compared with the classical models of Heisenberg [<i>Z. Physik</i>, 124, 628, (1948)], Obukhov [<i>Isv. Geogr. Geophys. Ser.</i>, 13, 58, (1949)] and the more detailed analysis of Tennekes and Lumley [<i>The First Course of Turbulence</i>, MIT press, (1972)]. The energy transfer statistics measured in the numerically simulated flows are found to be nearly self-similar for wavenumbers in the inertial range. Using the self-similar form measured within the limited scale range of the simulation, we construct an 'ideal' energy transfer function and the corresponding energy flux rate for an inertial range of infinite extent. From this flux rate we calculate the Kolmogorov constant to be 1.5, in excellent agreement with experiments [A.S. Monin and A.M. Yaglom, <i>Statistical Fluid Mechanics</i>, Vol. 2, MIT Press, (1975)].</p>				
14. SUBJECT TERMS isotropic turbulence, interacting scales, energy transfer		15. NUMBER OF PAGES 37	16. PRICE CODE A03	
17. SECURITY CLASSIFICATION OF REPORT Unclassified	18. SECURITY CLASSIFICATION OF THIS PAGE Unclassified	19. SECURITY CLASSIFICATION OF ABSTRACT	20. LIMITATION OF ABSTRACT	